ARTICLE OPEN

Check for updates

Quantum optimization within lattice gauge theory model on a quantum simulator

Zheng Yan [1,2 ✉], Zheng Zhou[3,4], Yan-Hua Zhou[5,6], Yan-Cheng Wang[7,8], Xingze Qiu[9 ✉], Zi Yang Meng [10 ✉] and Xue-Feng Zhang[5,6 ✉]

Simulating lattice gauge theory (LGT) Hamiltonian and its nontrivial states by programmable quantum devices has attracted numerous attention in recent years. Rydberg atom arrays constitute one of the most rapidly developing arenas for quantum simulation and quantum computing. The $\mathbb{Z}_2$ LGT and topological order has been realized in experiments while the $U(1)$ LGT is being worked hard on the way. States of LGT have local constraints and are fragmented into several winding sectors with topological protection. It is therefore difficult to reach the ground state in target sector for experiments, and it is also an important task for quantum topological memory. Here, we propose a protocol of sweeping quantum annealing (SQA) for searching the ground state among topological sectors. With the quantum Monte Carlo method, we show that this SQA has linear time complexity of size with applications to the antiferromagnetic transverse field Ising model, which has emergent $U(1)$ gauge fields. This SQA protocol can be realized easily on quantum simulation platforms such as Rydberg array and D-wave annealer. We expect this approach would provide an efficient recipe for resolving the topological hindrances in quantum optimization and the preparation of quantum topological state.

INTRODUCTION

Rydberg atom arrays constitute one of the most rapidly developing arenas for quantum simulation and quantum computing. They offer Ising-like interactions between qubits and single site manipulation, and also the ability to arrange hundreds of qubits in arbitrary geometry. This also opens up remarkable opportunities for studying topological phases of matter with fractional excitations. Recent quantum simulation advances have provided remarkable microscopic access to the quantum correlations of a $\mathbb{Z}_2$ quantum spin liquid (QSL)[1,2]. The $\mathbb{Z}_2$ QSL[3,4] is the simplest quantum state in two spatial dimensions with fractionalized excitations and time-reversal symmetry, and has the same anyon content as the toric code[5]. One of the most interesting directions in quantum simulation is to construct lattice gauge theory (LGT) Hamiltonian and its nontrivial quantum states via Rydberg arrays, superconducting circuits and other platforms[1,2,6–8]. Quantum dimer model as a typical LGT is widely prepared in certain highly frustrated parameter regions of Rydberg arrays[9–16]. LGT models have Hilbert space fragmentation due to the local constraints, the sub-Hilbert spaces are labeled by different winding numbers and protected by topological defects. The topological defects also induce nontrivial phenomena, such as incommensurate phases and Cantor deconfinement[17,18]. For example, in the incommensurate phase, each topological sector becomes the ground state in turn while tuning the parameter. In the thermodynamic limit, it means infinite topological sectors one by one arise as the ground state in a finite region of parameter, which is also called 'devil stairs'[19,20]. But it is a hardcore problem in experiment to make the state of the system changed from one sector to another while tuning related parameters, because the

topology always hinders the jumping between different sectors. At present, there is no control scheme of experiment that can overcome the topological protection and prepare/search quantum states in a certain topological sector accurately. On the other hand, quantum annealing (QA) method is a powerful tool for optimization of Ising-like encoded Hamiltonian[21–28], which utilizes the quantum fluctuation to approach the ground state. The degree of quantum acceleration depends very much on the design of QA algorithm[29–32], especially for the lattice gauge model[33]. Following recent technological advancements in manufacturing coupled qubit systems, the QA algorithm can be embedded into superconducting flux qubits[34–36]. Currently, QA computers, i.e., quantum annealers have also been commercialized, such as the D-wave machine, and it does show higher efficiency than classical computers in certain optimization problems[37–41]. Recently, Rydberg array simulator can even realize the Ising-like encoded Hamiltonian on a large scale with high tunability[1,2], which is thus an ideal QA implementation platform.

The normal optimization problems usually find the ground states of the glassy Hamiltonian as Fig. 1a. In this field, the technology has been developed very well and matured[21–28,42]. As the fast development of quantum control and simulation, especially recent Rydberg arrays experiments, the optimization problem of LGT Hamiltonian takes another hardcore problems of simulation [Fig. 1b], that is, how to reach the target topological sector containing the ground state. As mentioned in the introduction, for instance, the simulation of 'devil stairs' phenomenon requires the system can approach the ground states within different sectors under different parameters. As the complex topological defects that emerged in LGT systems are robust to

[1]Department of Physics, School of Science, Westlake University, Hangzhou, China. [2]Institute of Natural Sciences, Westlake Institute for Advanced Study, Hangzhou, China. [3]Perimeter Institute for Theoretical Physics, Waterloo, ON, Canada. [4]Department of Physics and Astronomy, University of Waterloo, Waterloo, ON, Canada. [5]Department of Physics, and Center of Quantum Materials and Devices, Chongqing University, Chongqing, China. [6]Chongqing Key Laboratory for Strongly Coupled Physics, Chongqing University, Chongqing, China. [7]Zhongfa Aviation Institute of Beihang University, Hangzhou, China. [8]Tianmushan Laboratory, Hangzhou, China. [9]School of Physics Science and Engineering, Tongji University, Shanghai, China. [10]Department of Physics and HKU-UCAS Joint Institute of Theoretical and Computational Physics, The University of Hong Kong, Hong Kong, China. ✉email: zhengyan@westlake.edu.cn; xingze@tongji.edu.cn; zymeng@hku.hk; zhangxf@cqu.edu.cn
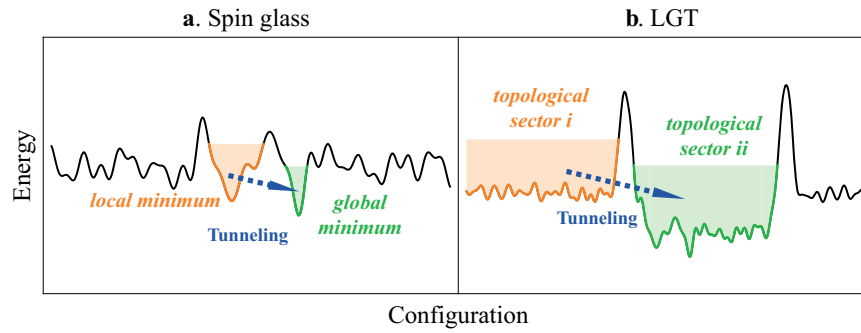
Fig. 1 Energy-Configuration landscape. Conventional optimization problems in glassy systems **a** and topological optimization problems in lattice gauge theory (LGT) cases **b**.
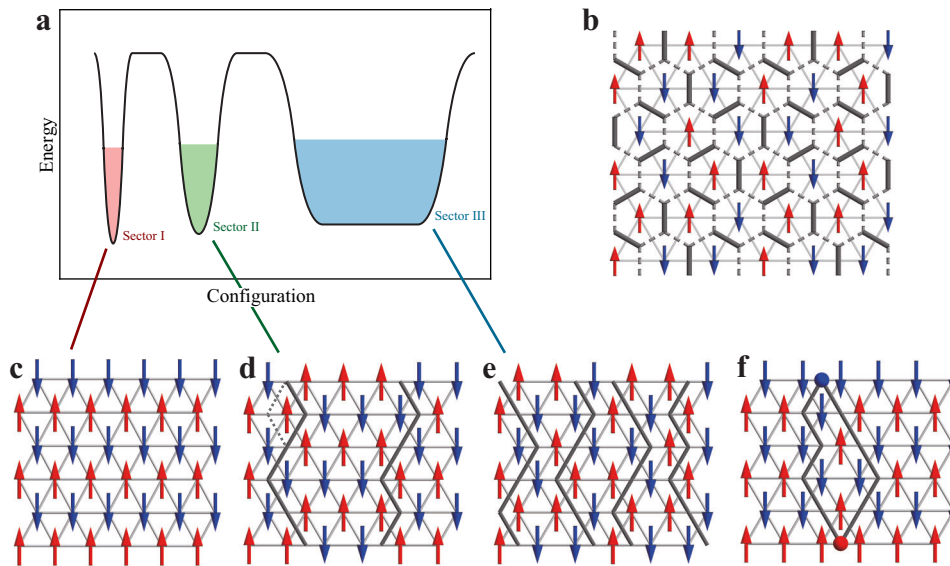

Fig. 2 The emergent topology in the triangular lattice AFM Ising model. a The schematic diagram for energy configurations of different topological sectors (with the three hardcore characteristics discussed in the main text). **b** The mapping between the constrained spin configuration and the dimers. **c** The stripe phase with no defect is the ground state of Hamiltonian Eq. (1) in $N_D = 0$ topological sector. **d**, **e** are the topological sector with $N_D = 2$ and $N_D = 4$ and the topological defects are denoted by the black lines. As shown in **d**, spin on corner can be flipped without breaking the 'triangle rule'. The defect before/after spin flipped is labeled by solid/dashed line. **f** A pair of spinons (triangle with 3 parallel spins) connected with defects. The spinons can be considered as local defects and they can annihilate (with local flipping) when meet.

quantum fluctuations, it is realized that these emergent topological structures could deeply hinder the efficiency of the existing annealing algorithms. Therefore it is the time of finding useful quantum annealing schemes for such systems, hereby, we give a powerful scheme, sweeping quantum annealing (SQA), to solve the problems. Different from the normal QA with local tunneling on each site, the SQA removes the topological defects by additional global annealing on virtual edges to overcome the barrier between the topological sectors. We demonstrate the effectiveness of SQA through some extremely egregious examples which can be realized in Rydberg experiments.

RESULTS

Model

Without losing generality, we use U(1) LGT as an example to test the efficiency of the different QA algorithms. Because 2+1d $U(1)$ LGT has about L^2 topological sectors, more than $\mathbb{Z}_2$ LGT which has only four sectors[12,43]. Moreover, we would design a hard-mode case to demonstrate the power of SQA. The difficult topological optimization problem has three characteristics as shown in Fig. 2a: (1) The minimum energies of many topological sectors are nearly

equal. (2) The target topological sector containing the ground state occupies small Hilbert subspace, it is difficult to be found. (3) Larger topological sectors provide enough degree of freedom for quantum fluctuations in the annealing process to compete with the ground energy sector. In other words, annealing tends to pull the system into the wrong sector for a kinetic energy advantage. Therefore, we consider such a frustrated antiferromagnetic (AF) Ising model with small transverse field on a triangular lattice, whose Hamiltonian reads

$$H_A = J_x \sum_{\langle ij \rangle_x} \sigma_i^z \sigma_j^z + J_\wedge \sum_{\langle ij \rangle_\wedge} \sigma_i^z \sigma_j^z - \delta \sum_i \sigma_i^x, \quad (1)$$

where σ^z and σ^x are the Pauli operator, $\langle ij \rangle_x$ and $\langle ij \rangle_\wedge$ represent the nearest-neighbor sites on the horizontal bonds and the interchain bonds, respectively, and J_x and $J_\wedge$ are the corresponding coupling strength. The emergent LGT in this model requires the $\delta \ll J_x, J_\wedge$. The emergent $U(1)$ gauge fields and topological properties in this model have been well-studied[44–48]. Due to the antiferromagnetic interaction, every triangle must be composed of two parallel and one antiparallel spins in the low-energy Hilbert space. We dub this local constraint as 'triangle rule", and the constraint-satisfying Hilbert space can be exactly mapped to a familiar quantum dimer

model[10,11,43,49–51]. Figure 2b shows this mapping between the constrained spin configuration on triangular lattice and the dimer configuration on the dual honeycomb lattice, where the bond with two parallel spins corresponds to a dimer. The dimer density on the honeycomb lattice can be understood as lattice electric field on the dual bond, and the local constraint can be written as the divergenceless condition. There thus emerges an $U(1)$ gauge field in this triangular AF Ising model[44,48,52], and the many-body configurations with constraints can be mapped to lattice electromagnetic fields which are naturally classified into different topological sectors[44]. Recent numerical works[48,53], which studied a triangular lattice AFM Ising model with small transverse field ($\delta \ll J$), have demonstrated that the parameter range of Eq.(1) is very close to the famous Rokhsar-Kivelson point and incommensurate phase with Cantor deconfinement of a general quantum dimer model on honeycomb lattice. To demonstrate the power of our algorithm, we put the Hamiltonian on a periodic boundary lattice, in which case the topological defects are much more robust.

Topological sectors are robust to quantum fluctuations emerged in the LGT systems and can be labeled by the number of topological defects N_D[48,54–56]. As examples, we show the spin configurations in different topological sectors in Fig. 2c–e for $N_D = 0, 2, 4$, respectively, if we set the stripe configurations [Fig. 2c] as the $N_D = 0$ reference state. Note that all these topological sectors are degenerate when $J_x = J_\wedge$ and $\delta = 0$, we thus set $J_x = 0.9J_\wedge$ and $\delta \ll J_\wedge - J_x$ in the following to break the degeneracy weakly and make the stripe configuration [Fig. 2c] with $N_D = 0$ has the lowest energy. This setting is for satisfying the hardcore three characteristics mentioned above, as shown in Fig. 2a. In fact, we can also set different configuration with target N_D as ground state via changing the related couplings J_i of bond i.

The ground state stripe phase in Fig. 2c is composed of horizontal bonds connecting parallel spins and interchain bonds connecting antiparallel spins. Without breaking the local constraint of the 'triangle rule', the number of horizontal antiparallel bonds is conserved in each row, and linking such antiparallel bonds on different chains will construct the one-dimensional global (topological) defect [Fig. 2d, e]. Note that there can be a mass of spin configurations for the same defect number, and the topological sectors thus have extensive nearly degenerate quantum states. In fact, the degeneracy is because flipping the spins at the corners of defects obeys the 'triangle rule' with little energy cost, as shown in Fig. 2d. Therefore, the degeneracy (degree of freedom) increases exponentially with the defect number N_D[12,43,48,51]. Changing the defect number requires generating a pair of spinons (constraint-breaking triangles) connected by defects [Fig. 2f], letting them go around the connected boundary to meet and annihilate. Such process changes N_D by two. However, exciting spinons and pulling them apart is extremely hard due to the large energy cost and global topology constraints, so it is difficult to achieve the ground-state energy sector from higher energy ones in this way.

Moreover, in the triangle rule limit ($\delta \ll J_x, J_\wedge$), the $J_\wedge - J_x > 0$ make the system favor stripe phase without topological defect while the $\delta \Sigma^x$ term favors more topological defects with flippable corners. The sector with many topological defects, which has much more freedom degree as the 'Sector III' of Fig. 2a shown, is easy to reach. Of course, we could set the 'Sector III' as the sector where the ground state in, but it seems trivial for an optimization problem because it is very easy to be found. Thus we set $\delta \ll J_\wedge - J_x$ in the following ($\delta = 0$ for simplicity), i.e., the ground state is stripe as the 'Sector I' of Fig. 2a shown. Although the target state is a classical state, it doesn't lose the generality because the key point here is to jump among different topological sectors while the details of the ground state is not important. Our choice aims increasing the coefficient of difficulty of such optimization.

Sweeping quantum annealing scheme

We first consider the conventional quantum annealing protocol, whose dynamics is generated by a Hamiltonian of the form

$$H_{QA} = H_A - h(t)\sum_i \sigma_i^x, \qquad (2)$$

where σ^x is the Pauli-x operator. The annealing schedule is controlled by linearly reducing the transverse field $h(t)$ from a sufficiently large initial value $h(0) = 5J_\wedge$ to the final value $h(\tau) = 0$, so that the original Ising Hamiltonian H_A is recovered at the end.

In order to obtain the numerical results with large system size, we adopt the stochastic series expansion (SSE) method within a continuous time frame[57–61] to resolve the quantum dynamics, which essentially belongs to the quantum Monte Carlo (QMC) simulation[62]. The QMC can reveal the scaling behaviors of QA as same as real-time simulations and has been widely used to study the annealing problems[63–70]. We use the Monte Carlo step (MCS) to label the annealing time. One MCS is defined as visiting all the spins, so it is proportional to size L^2. However, as shown in Fig. 3a, the QA protocol can not reach the ground state even for long enough evolution time.

We have also tried the quantum annealing with inhomogeneous transverse field, i.e., $H_{QA-h} = H_A + \sum_i h_i(t)\sigma_i^x$ with site-dependent random field $h_i(t)$, which is initially chosen from the uniform distribution $[0, 10J_\wedge]$, and then linearly reduced to 0. We denote such annealing as 'QA-h', which is suggested to weaken the effect of second-order phase transition and improve the efficiency of quantum annealing[71–75]. Nevertheless, as shown in Fig. 3a, it behaves most like the conventional QA protocol and cannot improve efficiency.

The inefficiency of the above two QA protocols can be attributed to the following aspects. If the σ^x breaks the 'triangle rule', it will take a huge energy cost of about $2J_\wedge$ which is forbidden at low temperature. Thus, the σ^x operators always flip the spins at the corners of defects without Ising energy costs [Fig. 2d] and obtain extra kinetic energy advantage of the σ^x term at the same time. All these low-energy actions can not change the number of topological defects (i.e., the number of topological sectors), but just twist the corner by flipping the spin on it, such as the red spin of Fig. 2d, after flipping the spin the corner on the right side will be turned to left as shown by the dashed line. Therefore, the fluctuations introduced by both QA and QA-h can only deform the defects but cannot create/annihilate them. However, topological optimization problems usually involve non-local excitations and require global operations.

In essence, the optimization problem here is an annealing problem to find the optimal topological sectors in Fig. 2a. In this case, the number of states in a topological sector increases with the defect number N_D, so the stripe configuration of the ground state is the smallest sector and hard to be reached in Hilbert space as one needs an annealing algorithm that can both tunnel through different topological sectors and reduce the energy.

In order to obtain non-local excitations to surmount the problem of the topological defects, we develop sweeping quantum annealing to achieve the ground state topological sector. The key point is the topological defects can be moved out continuously through the 'open edge' by local operators. Thus the system can easily reach the global minimum intuitively if we can change the boundary condition during annealing. The schematic diagram of SQA on a torus lattice taking square lattice as an example is shown in Fig. 3b. The feasible algorithmic scheme on a quantum annealing platform is to do additional annealing with a large transverse field on a virtual edge as the purple circle of Fig. 3b shown. Intuitively, a large transverse field can polarize the spin to the x-axis, acting as if shearing the Ising coupling bond apart. As shown in the right part of Fig. 3b, the central spin has been polarized to reduce its Ising interaction with other spins. A great
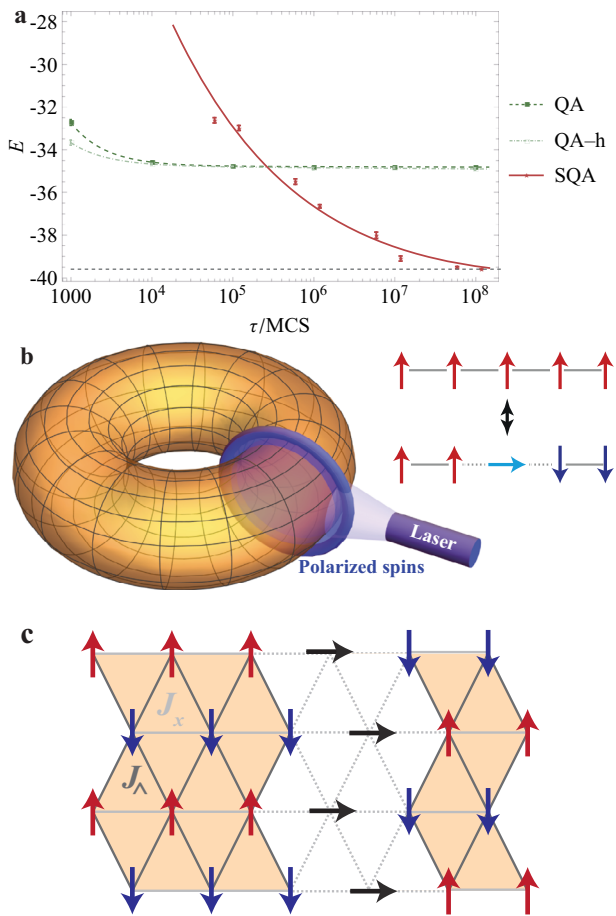
Fig. 3 **The sweeping quantum annealing. a** The energy is computed for 6×6 system and the true ground state energy $E_g = -39.6 J_\wedge$ is denoted by the gray dashed line. The expectation value of E and its error bars are obtained from averaging over 64 independent annealing runs. The straightforward QA and QA-h have the worst annealing performance, the best among these is the SQA. In the whole paper, we use the statistical error to define the error bar, i.e., $\sigma / \sqrt{N_{sampling}}$, where the σ is the standard error and $N_{sampling}$ is the number of QMC samplings. **b** Schematic diagram of SQA on a torus square lattice. We perform additional quantum annealing on 'virtual edges' of the system to reduce the topological defects. In quantum simulation experiments, the global transverse field term can be controlled with tunable laser or arbitrary waveform generators[86–88]. **c** The SQA schematic diagram on a triangular lattice with the periodic boundary condition along both x and y directions. The polarized spins lose the Ising interactions which is similar to opening the boundary, as the white region shown.

advantage is that the strength of the transverse field can be easily and continuously adjusted by tunning the Rabi frequency of the laser in the experiment. Similarly, the SQA on the triangular lattice is shown in Fig. 3c, all the spins on the virtual edge are polarized, which is equal to opening the edge effectively.

We then scan all the virtual edges one by one in turn along a certain direction with strongly annealing transverse field, which is expected to achieve the effect across topological sectors. The specific plan is as follows: (1) Keep the conventional quantum annealing process on every site as mentioned above, that is, linearly decreasing the h slowly down from $h(0)$ zero. (2) Divide the whole process into L (system length) parts. In every part, add a extra strong transverse field (as same as $h(0)$) on virtual edges in order and reduce the field strength slowly to $h(t)$. $h(t)$ is the field strength of the traditional QA at the end of this part. Then move to the next virtual edge and repeat the same process until all the
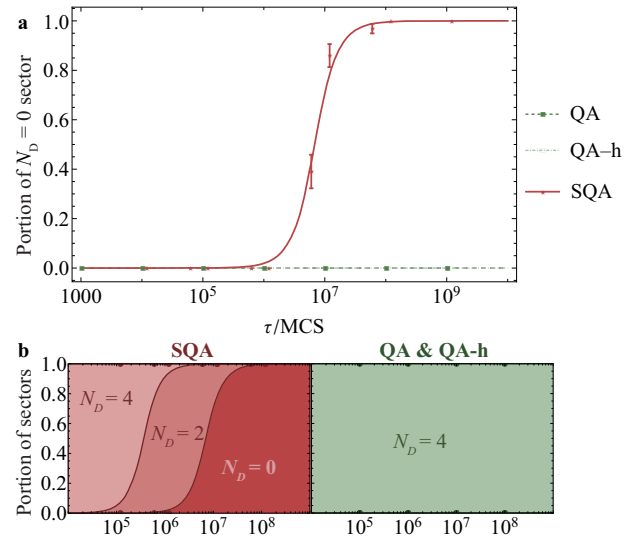

Fig. 4 **The topological sector changes only by SQA. a** The proportion of ground state sector as a function of the annealing time with different methods. **b** The proportion of all topological sectors as a function of the annealing time with different methods.

edges ($1 \sim L$) are visited. From Fig. 3a, we can see an obvious advantage of SQA to arrive at the ground state quickly. The detailed pseudo-code protocol of SQA is shown in Supplemental Note 2.

The physical reason for the superior behavior of SQA in the topological frustrated optimization problem is that it effectively removes topological defects in the systematic sweeping. As demonstrated in Fig. 4a, different from the QA and QA-h, the proportion of ND = 0 sectors increases with the annealing time of SQA. Furthermore, the proportion of different topological sectors is shown in Fig. 4b. The conventional QA and QA-h are stuck in $N_D = 4$ sectors, which reveals the reason for their inefficiency. Clearly, the best of all annealing schemes is the SQA which can straightforwardly change the topology of the system at any position. In order to strengthen the evidence of the effectiveness and universality of SQA, we simulate another difficult topological optimization problem of a fully frustrated Ising system on the square lattice (corresponding to the square lattice quantum dimer model) in Supplementary Note 4, where we see that our SQA protocol is also efficient.

Remarkably, our SQA protocol can prepare the target topological state at a time that scales linearly with the system size ($N = L^2$). Figure 5 shows the energy per site E/N as a function of MCS, in which every MCS is defined with scaling as L^2, i.e., $1 MCS \sim L^2$. We see that the lines almost coincide with each other for different system size, which clearly demonstrates a linear increase of annealing time with the system size, since the annealing time is proportional to MCS[67–70]. The power cost for the algorithm is a strong advantage.

In addition, we have also discussed the effect of thermal annealing (TA)[76,77] in Supplementary Note 6 although it is almost impossible to realize in the recent cold atom experiments. Hopefully, the result may inspire related experiments in the future.

Experimental candidates

The experimental candidates for implementing the SQA protocol are many, for example in the superconducting circuits[1,78–80]. We find SQA is in particular applicable to the Rydberg arrays, which have recently been utilized to simulate the $\mathbb{Z}_2$ quantum spin liquid[2].
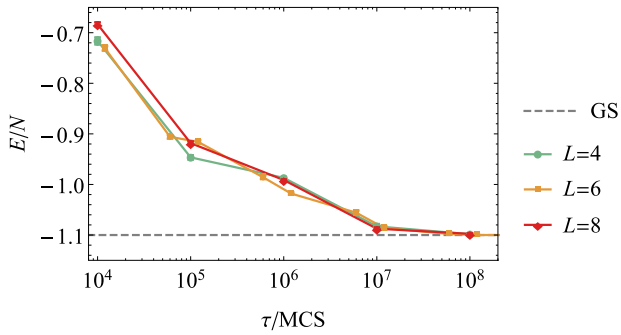
Fig. 5 Time complexity. The energy per site E/N is computed for 4×4, 6×6 and 8×8 systems and the true ground state energy per site is denoted by the dashed line. The expectation value of E/N and its error bars are obtained from averaging over 64 independent annealing runs. It shows a good convergence for all sizes. One MCS is defined as visiting all the spins, so MCS scales as L^2.

Below we discuss in detail the Rydberg arrays systems are the idea platform to simulate the $U(1)$ LGT model [see Eq. (1)] and implement the SQA protocol. The effective Hamiltonian of Rydberg arrays is[81,82]

$$H_R = h \sum_i \sigma_i^x - \mu \sum_i n_i + V \sum_{i>j} \frac{n_i n_j}{|i-j|^6}, \qquad (3)$$

where i and j are the site labels, $n_i = 0, 1$ is the density operator to probe the ground state or Rydberg state, respectively, and σ^x is the tunneling term (Pauli-x operator) to connect the two states. We can use the spin-1/2 language to describe the qubit within the two-level Rydberg system, since there is a common mapping between the hardcore boson and spin, that is, $n = (\sigma^z + 1)/2$ and ground/Rydberg state corresponds to spin down/up state.

The Rydberg arrays Hamiltonian [Eq. (3)] on the triangular lattice can then be cast into the form of [Eq. (2)] with emergent $U(1)$ LGT, it has been realized in experiment in fact[83]. Firstly, since the repulsive interaction decays very fast, i.e., $1/r^6$, the strength of the second nearest neighbors on triangular lattice is about 0.037 compared with that of the first neighbor, so the model can be further simplify as $H_R = h \sum_i \sigma_i^x - \mu \sum_i n_i + V \sum_{\langle ij \rangle} n_i n_j$ with only nearest neighbors. Then, we set $\mu = V$ and use $n_i = 2\sigma_i^z + 1$ to simplify the Hamiltonian in σ operator form as $H_R = h \sum_i \sigma_i^x + \frac{V}{4} \sum_{\langle ij \rangle} \sigma_i^z \sigma_j^z$. Lastly, set the distances of Rydberg atoms along x-axis a little farther than along other directions, and then the anisotropy Hamiltonian in Eq. (2), $H_R = h \sum_i \sigma_i^x + \frac{V_\triangle}{4} \sum_{\langle ij \rangle_\triangle} \sigma_i^z \sigma_j^z + \frac{V_x}{4} \sum_{\langle ij \rangle_x} \sigma_i^z \sigma_j^z$, is obtained. In this way, the superior behavior of SQA we have discussed for Eq. (2), can be readily applied to the Rydberg arrays, and all the parameters can be tuned by adjusting laser detuning or Rabi frequency. For the experimental sources of error, the main decay channels of the Rydberg states include blackbody radiation-induced errors and spontaneous radiative decay transitions to lower-lying states[84]. In order to mitigate them, several hardware-efficient and fault-tolerant quantum computation schemes has been proposed[85]. We therefore think it has well experimental feasibility to implement our SQA protocol on the present Rydberg atom array platform.

DISCUSSION

With the fast development of Rydberg arrays simulation, precise regulation of the quantum state of LGT within the topological sector is required. For such topological optimization problems, there is still a lack of systematic quantum simulation protocol. In this work, we find that the emergent topological properties in frustrated Ising systems greatly reduce the efficiency of both conventional thermal and quantum annealing. Borrowing the idea of changing topology by cutting and gluing the system, we invent such a generalized algorithm—the sweeping quantum annealing method to solve these problems with huge quantum speedup. Moreover, the SQA can be easily implemented in realistic quantum simulation experimental platforms because the global transverse field term can be controlled finely by tunable laser or arbitrary waveform generators[78–80,86–91]. After comparing with conventional quantum and sweeping quantum annealing algorithm, we find that the SQA presents high efficiency and validity while other annealing schemes fail. The sweeping quantum annealing therefore opens up an effective and innovative way for controlling the quantum states of LGT. It will also be of interest to study the effectiveness of SQA under noises and dissipations[92,93] which commonly exist in the quantum simulator.

It's worth noting that the topological defects are in one direction in this work. Topological defects along the other direction can also be removed under the SQA along that direction. Therefore, the system with defects in both directions can be optimized by SQA mixed in both directions in principle. In future works, more general systems with both nearly degenerate topological sectors in two directions and glassy minimums will be discussed.

METHODS

Quantum Monte Carlo simulation

We use the continuous-time quantum Monte Carlo method for the quantum annealing in this paper. Because the discrete-time QMC may take the opposite result due to the error[67]. The temperature $T = 1/\beta$ we set is $J_\triangle/20$, which is much smaller than the energy scale of spinon excitation $\sim 2J_\triangle$. The temperature can keep the configurations obeying the 'triangle rule' with emergent LGT. The dynamic of annealing can be simulated via QMC because the time scaling of QMC is the same as real-time evolution, these simulations have been widely used to study the quantum annealing behaviors[67–70].

The QMC we used is a stochastic series expansion (SSE) algorithm[57–59]. The partition function Z is dealt with a Taylor expansion as:

$$Z = \sum_\alpha \sum_{n=0}^\infty \frac{\beta^n}{n!} \langle \alpha | (-H)^n | \alpha \rangle \qquad (4)$$

Then we extract the wanted information via sampling these configurations of Taylor expansion. More details of quantum Monte Carlo simulations for QA, QA-h, and SQA have been explained in Supplementary Note 1.

DATA AVAILABILITY

The data that support the findings of this study are available from the authors upon reasonable request.

CODE AVAILABILITY

The code is available from the authors upon reasonable request.

REFERENCES

1. Satzinger, K. J. et al. Realizing topologically ordered states on a quantum processor. *Science* **374**, 1237–1241 (2021).
2. Semeghini, G. et al. Probing topological spin liquids on a programmable quantum simulator. *Science* **374**, 1242–1247 (2021).
3. Read, N. & Sachdev, S. Large-N expansion for frustrated quantum antiferromagnets. *Phys. Rev. Lett.* **66**, 1773–1776 (1991).

4. Wen, X. G. Mean-field theory of spin-liquid states with finite energy gap and topological orders. *Phys. Rev. B* **44**, 2664–2672 (1991).

5. Kitaev, A. Fault tolerant computation by anyons. *Ann. Phys.* **303**, 2–30 (2003).

6. Li, K. et al. Experimental identification of non-abelian topological orders on a quantum simulator. *Phys. Rev. Lett.* **118**, 080502 (2017).

7. Lumia, L. et al. Two-dimensional z_2 lattice gauge theory on a near-term quantum simulator: variational quantum optimization, confinement, and topological order. *PRX Quantum* **3**, 020320 (2022).

8. Yan, Z., Wang, Y.-C., Samajdar, R., Sachdev, S. & Meng, Z. Y. Emergent glassy behavior in a kagome Rydberg atom array. *Phys. Rev. Lett.* **130**, 206501 (2023).

9. Rokhsar, D. S. & Kivelson, S. A. Superconductivity and the quantum hard-core dimer gas. *Phys. Rev. Lett.* **61**, 2376–2379 (1988).

10. Yan, Z. et al. Widely existing mixed phase structure of the quantum dimer model on a square lattice. *Phys. Rev. B* **103**, 094421 (2021).

11. Yan, Z., Wang, Y.-C., Ma, N., Qi, Y. & Meng, Z. Y. Topological phase transition and single/multi anyon dynamics of z2 spin liquid. *npj Quantum Mater.* **6**, 39 (2021).

12. Moessner, R. & Raman, K. S. Quantum dimer models. In *Introduction to Frustrated Magnetism*, 437–479 (Springer, 2011).

13. Yan, Z., Samajdar, R., Wang, Y.-C., Sachdev, S. & Meng, Z. Y. Triangular lattice quantum dimer model with variable dimer density. *Nat. Commun.* **13**, 5799 (2022).

14. Yan, Z. et al. Fully packed quantum loop model on the triangular lattice: Hidden vison plaquette phase and cubic phase transitions. Preprint at https://arxiv.org/abs/2205.04472 (2022).

15. Zhou, Z., Yan, Z., Liu, C., Chen, Y. & Zhang, X.-F. Quantum simulation of two-dimensional U(1) gauge theory in Rydberg atom arrays. Preprint at https://arxiv.org/abs/2212.10863 (2022).

16. Ran, X. et al. Fully packed quantum loop model on the square lattice: phase diagram and application for Rydberg atoms. *Phys. Rev. B* **107**, 125134 (2023).

17. Fradkin, E., Huse, D. A., Moessner, R., Oganesyan, V. & Sondhi, S. L. Bipartite Rokhsar–Kivelson points and cantor deconfinement. *Phys. Rev. B* **69**, 224415 (2004).

18. Schlittler, T., Barthel, T., Misguich, G., Vidal, J. & Mosseri, R. Phase diagram of an extended quantum dimer model on the hexagonal lattice. *Phys. Rev. Lett.* **115**, 217202 (2015).

19. von Boehm, J. & Bak, P. Devil's stairs and the commensurate-commensurate transitions in cesb. *Phys. Rev. Lett.* **42**, 122–125 (1979).

20. Bak, P. Commensurate phases, incommensurate phases and the devil's staircase. *Rep. Prog. Phys.* **45**, 587 (1982).

21. Fu, Y. & Anderson, P. W. Application of statistical mechanics to NP-complete problems in combinatorial optimisation. *J. Phys. A* **19**, 1605–1620 (1986).

22. Mezard, M., Parisi, G. & Virasoro, M. *Spin Glass Theory and Beyond* (World Scientific, 1986). https://doi.org/10.1142/0271.

23. Huse, D. A. & Fisher, D. S. Residual energies after slow cooling of disordered systems. *Phys. Rev. Lett.* **57**, 2203–2206 (1986).

24. Santoro, G. E., Martoňák, R., Tosatti, E. & Car, R. Theory of quantum annealing of an Ising spin glass. *Science* **295**, 2427–2430 (2002).

25. Lucas, A. Ising formulations of many NP problems. *Front. Phys.* **2**, 5 (2014).

26. Kadowaki, T. & Nishimori, H. Quantum annealing in the transverse ising model. *Phys. Rev. E* **58**, 5355 (1998).

27. Mezard, M. & Montanari, A. *Information, physics, and computation* (Oxford University Press, 2009).

28. Heim, B., Rønnow, T. F., Isakov, S. V. & Troyer, M. Quantum versus classical annealing of Ising spin glasses. *Science* **348**, 215–217 (2015).

29. Somma, R. D., Nagaj, D. & Kieferová, M. Quantum speedup by quantum annealing. *Phys. Rev. Lett.* **109**, 050501 (2012).

30. Das, A. & Chakrabarti, B. K. *Quantum annealing and related optimization methods*, vol. 679 (Springer Science & Business Media, 2005).

31. Das, A. & Chakrabarti, B. K. Colloquium: Quantum annealing and analog quantum computation. *Rev. Mod. Phys.* **80**, 1061–1081 (2008).

32. Ebadi, S. et al. Quantum optimization of maximum independent set using Rydberg atom arrays. *Science* **376**, 1209–1215 (2022).

33. Giudici, G., Lukin, M. D. & Pichler, H. Dynamical preparation of quantum spin liquids in Rydberg atom arrays. *arXiv preprint arXiv:2201.04034*. https://arxiv.org/abs/2201.04034 (2022).

34. Johnson, M. W. et al. Quantum annealing with manufactured spins. *Nature* **473**, 194–198 (2011).

35. Boixo, S., Albash, T., Spedalieri, F. M., Chancellor, N. & Lidar, D. A. Experimental signature of programmable quantum annealing. *Nat. Commun.* **4**, 1–8 (2013).

36. Boixo, S. et al. Evidence for quantum annealing with more than one hundred qubits. *Nat. Phys.* **10**, 218–224 (2014).

37. Perdomo-Ortiz, A., Dickson, N., Drew-Brook, M., Rose, G. & Aspuru-Guzik, A. Finding low-energy conformations of lattice protein models by quantum annealing. *Sci. Rep.* **2**, 571 (2012).

38. Novotny, M., Hobl, Q. L., Hall, J. & Michielsen, K. Spanning tree calculations on d-wave 2 machines. *J. Phys.: Conf. Ser.* **681**, 012005 (2016).

39. Qiu, X., Zou, J., Qi, X. & Li, X. Precise programmable quantum simulations with optical lattices. *npj Quantum Inf.* **6**, 87 (2020).

40. Qiu, X., Zoller, P. & Li, X. Programmable quantum annealing architectures with Ising quantum wires. *PRX Quantum* **1**, 020311 (2020).

41. King, A. D. et al. Quantum critical dynamics in a 5,000-qubit programmable spin glass. *Nature* 1–6 (2023).

42. King, A. D. et al. Quantum annealing simulation of out-of-equilibrium magnetization in a spin-chain compound. *PRX Quantum* **2**, 030317 (2021).

43. Yan, Z. Global scheme of sweeping cluster algorithm to sample among topological sectors. *Phys. Rev. B* **105**, 184432 (2022).

44. Moessner, R. & Sondhi, S. L. Ising models of quantum frustration. *Phys. Rev. B* **63**, 224401 (2001).

45. Isakov, S. V. & Moessner, R. Interplay of quantum and thermal fluctuations in a frustrated magnet. *Phys. Rev. B* **68**, 104409 (2003).

46. Wang, Y.-C., Qi, Y., Chen, S. & Meng, Z. Y. Caution on emergent continuous symmetry: a Monte Carlo investigation of the transverse-field frustrated Ising model on the triangular and honeycomb lattices. *Phys. Rev. B* **96**, 115160 (2017).

47. Da Liao, Y. et al. Phase diagram of the quantum Ising model on a triangular lattice under external field. *Phys. Rev. B* **103**, 104416 (2021).

48. Zhou, Z., Liu, D.-X., Yan, Z., Chen, Y. & Zhang, X.-F. Quantum tricriticality of incommensurate phase induced by quantum strings in frustrated Ising magnetism. *SciPost Phys.* **14**, 037 (2023).

49. Moessner, R. & Raman, K. S. Quantum Dimer Models, 437–479 (Springer Berlin Heidelberg, Berlin, Heidelberg, 2011). https://doi.org/10.1007/978-3-642-10589-0_17.

50. Yan, Z. et al. Sweeping cluster algorithm for quantum spin systems with strong geometric restrictions. *Phys. Rev. B* **99**, 165135 (2019).

51. Zhou, Z., Liu, C., Yan, Z., Chen, Y. & Zhang, X.-F. Quantum dynamics of topological strings in a frustrated ising antiferromagnet. *npj Quantum Mater.* **7**, 60 (2022).

52. Yan, Z., Meng, Z. Y., Huse, D. A. & Chan, A. Height-conserving quantum dimer models. *Phys. Rev. B* **106**, L041115 (2022).

53. Zhou, Z., Yan, Z., Liu, C., Chen, Y. & Zhang, X.-F. Emergent rokhsar-kivelson point in realistic quantum ising models. Preprint at https://arxiv.org/abs/2106.05518 (2021).

54. Zhang, X.-F. & Eggert, S. Chiral edge states and fractional charge separation in a system of interacting bosons on a kagome lattice. *Phys. Rev. Lett.* **111**, 147201 (2013).

55. Zhang, X.-F., Hu, S., Pelster, A. & Eggert, S. Quantum domain walls induce incommensurate supersolid phase on the anisotropic triangular lattice. *Phys. Rev. Lett.* **117**, 193201 (2016).

56. Zhang, X.-F., He, Y.-C., Eggert, S., Moessner, R. & Pollmann, F. Continuous easy-plane deconfined phase transition on the kagome lattice. *Phys. Rev. Lett.* **120**, 115702 (2018).

57. Sandvik, A. W. & Kurkijärvi, J. Quantum Monte Carlo simulation method for spin systems. *Phys. Rev. B* **43**, 5950–5961 (1991).

58. Sandvik, A. W. Stochastic series expansion method with operator-loop update. *Phys. Rev. B* **59**, R14157 (1999).

59. Sandvik, A. W. Stochastic series expansion method for quantum Ising models with arbitrary interactions. *Phys. Rev. E* **68**, 056701 (2003).

60. Sandvik, A. W. Stochastic series expansion methods. *arXiv preprint arXiv:1909.10591* (2019).

61. Desai, N. & Pujari, S. Resummation-based quantum monte carlo for quantum paramagnetic phases. *Phys. Rev. B* **104**. https://doi.org/10.1103/PhysRevB.104.L060406 (2021).

62. *The Monte Carlo simulation for QA, QA-h and SQA, the detailed implementations of SQA with the pseudo-codes, the example of fully frustrated Ising model on square lattice, are presented in the Supplemental Materials.*

63. De Grandi, C., Polkovnikov, A. & Sandvik, A. Universal nonequilibrium quantum dynamics in imaginary time. *Phys. Rev. B* **84**, 224303 (2011).

64. Liu, C.-W., Polkovnikov, A. & Sandvik, A. W. Quasi-adiabatic quantum Monte Carlo algorithm for quantum evolution in imaginary time. *Phys. Rev. B* **87**, 174302 (2013).

65. Liu, C.-W., Polkovnikov, A. & Sandvik, A. W. Dynamic scaling at classical phase transitions approached through nonequilibrium quenching. *Phys. Rev. B* **89**, 054307 (2014).

66. Liu, C.-W., Polkovnikov, A. & Sandvik, A. W. Quantum versus classical annealing: insights from scaling theory and results for spin glasses on 3-regular graphs. *Phys. Rev. Lett.* **114**, 147203 (2015).

67. Isakov, S. V. et al. Understanding quantum tunneling through quantum Monte Carlo simulations. *Phys. Rev. Lett.* **117**, 180402 (2016).

68. Denchev, V. S. et al. What is the computational value of finite-range tunneling? *Phys. Rev. X* **6**, 031015 (2016).

69. Jiang, Z. et al. Scaling analysis and instantons for thermally assisted tunneling and quantum Monte Carlo simulations. *Phys. Rev. A* **95**, 012322 (2017).

70. King, A. D. et al. Scaling advantage over path-integral Monte Carlo in quantum simulation of geometrically frustrated magnets. *Nat. Commun.* **12**, 1–6 (2021).

71. Suzuki, S., Nishimori, H. & Suzuki, M. Quantum annealing of the random-field Ising model by transverse ferromagnetic interactions. *Phys. Rev. E* **75**, 051112 (2007).

72. Zurek, W. H. & Dorner, U. Phase transition in space: how far does a symmetry bend before it breaks? *Philos. Trans. R. Soc. A* **366**, 2953–2972 (2008).

73. Dziarmaga, J. & Rams, M. M. Adiabatic dynamics of an inhomogeneous quantum phase transition: the case of a $z > 1$ dynamical exponent. *N. J. Phys.* **12**, 103002 (2010).

74. Rams, M. M., Mohseni, M. & del Campo, A. Inhomogeneous quasi-adiabatic driving of quantum critical dynamics in weakly disordered spin chains. *N. J. Phys.* **18**, 123034 (2016).

75. Hauke, P., Katzgraber, H. G., Lechner, W., Nishimori, H. & Oliver, W. D. Perspectives of quantum annealing: methods and implementations. *Rep. Prog. Phys.* **83**, 054401 (2020).

76. Brooke, J., Bitko, D., Rosenbaum, F. T. & Aeppli, G. Quantum annealing of a disordered magnet. *Science* **284**, 779–781 (1999).

77. Brooke, J., Rosenbaum, T. & Aeppli, G. Tunable quantum tunnelling of magnetic domain walls. *Nature* **413**, 610–613 (2001).

78. Wang, Z. et al. Observation of emergent $\mathbb{Z}_2$ gauge invariance in a superconducting circuit. *Phys. Rev. Res* **4**, L022060 (2022).

79. Ge, Z.-Y., Huang, R.-Z., Meng, Z.-Y. & Fan, H. Quantum simulation of lattice gauge theories on superconducting circuits: Quantum phase transition and quench dynamics. *Chin. Phys. B* **31**, 020304 (2022).

80. Xu, K. et al. Probing dynamical phase transitions with a superconducting quantum simulator. *Sci. Adv.* **6**, eaba4935 (2020).

81. Saffman, M., Walker, T. G. & Mølmer, K. Quantum information with Rydberg atoms. *Rev. Mod. Phys.* **82**, 2313–2363 (2010).

82. Browaeys, A. & Lahaye, T. Many-body physics with individually controlled Rydberg atoms. *Nat. Phys.* **16**, 132–142 (2020).

83. Scholl, P. et al. Quantum simulation of 2D antiferromagnets with hundreds of Rydberg atoms. *Nature* **595**, 233–238 (2021).

84. Beterov, I. I., Ryabtsev, I. I., Tretyakov, D. B. & Entin, V. M. Quasiclassical calculations of blackbody-radiation-induced depopulation rates and effective lifetimes of rydberg ns, np, and nd alkali-metal atoms with $n \leq 80$. *Phys. Rev. A* **79**, 052504 (2009).

85. Cong, I. et al. Hardware-efficient, fault-tolerant quantum computation with Rydberg atoms. *Phys. Rev. X* **12**, 021049 (2022).

86. Kim, K. et al. Quantum simulation of frustrated ising spins with trapped ions. *Nature* **465**, 590–593 (2010).

87. Kim, K. et al. Quantum simulation of the transverse ising model with trapped ions. *N. J. Phys.* **13**, 105003 (2011).

88. Georgescu, I. M., Ashhab, S. & Nori, F. Quantum simulation. *Rev. Mod. Phys.* **86**, 153 (2014).

89. Edwards, E. E. et al. Quantum simulation and phase diagram of the transverse-field ising model with three atomic spins. *Phys. Rev. B* **82**, 060412 (2010).

90. King, A. D. et al. Observation of topological phenomena in a programmable lattice of 1,800 qubits. *Nature* **560**, 456–460 (2018).

91. Endo, S., Sun, J., Li, Y., Benjamin, S. C. & Yuan, X. Variational quantum simulation of general processes. *Phys. Rev. Lett.* **125**, 010501 (2020).

92. Cai, Z., Schollwöck, U. & Pollet, L. Identifying a bath-induced bose liquid in interacting spin-boson models. *Phys. Rev. Lett.* **113**, 260403 (2014).

93. Yan, Z. et al. Interacting lattice systems with quantum dissipation: a quantum monte carlo study. *Phys. Rev. B* **97**, 035148 (2018).

AUTHOR CONTRIBUTIONS

Z.Y. and Z.Z. contributed equally to this work (co-first author). Z.Y., Z.Y.M. and X.F.Z. initiated the work. Z.Y. put forward the SQA scheme. Z.Y. and Z.Z. performed the QMC computational simulations. Y.H.Z. did the real-time evolution in small size. All authors contributed to the analysis of the results. X.Q., Z.Y.M. and X.F.Z. supervised the project.

COMPETING INTERESTS

The authors declare no competing interests.

ADDITIONAL INFORMATION

Supplementary information The online version contains supplementary material available at https://doi.org/10.1038/s41534-023-00755-z.

Correspondence and requests for materials should be addressed to Zheng Yan, Xingze Qiu, Zi Yang Meng or Xue-Feng Zhang.

Reprints and permission information is available at http://www.nature.com/reprints

Publisher's note Springer Nature remains neutral with regard to jurisdictional claims in published maps and institutional affiliations.